Traffic 2005; **6:** 1183–1195
Blackwell Munksgaard

doi: 10.1111/j.1600-0854.2005.00352.x

Biochemical and Crystallographic Studies Reveal a Specific Interaction Between TRAPP Subunits Trs33p and Bet3p

Min-Sung Kim[1], Min-Ju Yi[1], Kwang-Hoon Lee[1], John Wagner[2], Christine Munger[2], Yeon-Gil Kim[1], Malcolm Whiteway[3], Miroslaw Cygler[2,3], Byung-Ha Oh[1,*] and Michael Sacher[2,*]

[1]Center for Biomolecular Recognition, Department of Life Sciences and Division of Molecular and Life Sciences, Pohang University of Science and Technology, Pohang, Kyungbuk, 790-784, Korea
[2]Montreal Network for Proteomics and Department of Biochemistry, McGill University, 740 Dr Penfield Ave., Montreal, Quebec, Canada
[3]Biotechnology Research Institute, 6100 Royalmount Ave., Montreal, Quebec, Canada
**Corresponding authors: Michael Sacher, michael.sacher@bri.nrc.ca* and *Byung-Ha Oh, bhoh@postech.ac.kr*

Transport protein particle (TRAPP) comprises a family of two highly related multiprotein complexes, with seven common subunits, that serve to target different classes of transport vesicles to their appropriate compartments. Defining the architecture of the complexes will advance our understanding of the functional differences between these highly related molecular machines. Genetic analyses in yeast suggested a specific interaction between the TRAPP subunits Bet3p and Trs33p. A mammalian bet3–trs33 complex was crystallized, and the structure was solved to 2.2 Å resolution. Intriguingly, the overall fold of the bet3 and trs33 monomers was similar, although the proteins had little overall sequence identity. *In vitro* experiments using yeast TRAPP subunits indicated that Bet3p binding to Trs33p facilitates the interaction between Bet3p and another TRAPP subunit, Bet5p. Mutational analysis suggests that yeast Trs33p facilitates other Bet3p protein–protein interactions. Furthermore, we show that Trs33p can increase the Golgi-localized pool of a mutated Bet3 protein normally found in the cytosol. We propose that one of the roles of Trs33p is to facilitate the incorporation of the Bet3p subunit into assembling TRAPP complexes.

Key words: Bet3p, **Golgi**, **TRAPP**, **Trs33p**, **vesicle-tethering complex**

Received 9 August 2005, revised and accepted 9 September 2005, published on-line 6 October 2005

Ensuring that proteins and lipids are properly localized within a cell requires the involvement of many different factors. Some of the most upstream factors are believed to be vesicle-tethering complexes and long, rod-like proteins capable of forming coiled-coils (1–5). The vesicle-tethering complexes include the exocyst (6), VFT/GARP (7,8), COG (9), class C/HOPS (10–12) and the transport protein particle (TRAPP) I and II complexes (13,14). While the exact mechanism by which these complexes function in the secretory pathway is not known, they have all been reported to interact with Rab GTPases either as effectors or as guanine nucleotide exchange factors (15–19).

Each of the vesicle-tethering complexes, or several components of the complexes, localizes to a distinct intracellular compartment. These include the plasma membrane (exocyst), the *trans*-Golgi (VFT/GARP), the endosome (class C/HOPS), the Golgi (COG) and an early Golgi compartment (TRAPP complexes) (7–9,11,12,20–22). Because these complexes are believed to be one of the first factors encountered by the vesicle (23), a stringent mechanism must be in place to ensure that they are properly localized. Such mechanisms are presently unknown and may vary among the different complexes. Recently, the crystal structure of the murine bet3 subunit of TRAPP has provided some clues as to how this vesicle tether localizes to the Golgi (24,25). The protein forms a homodimer containing (i) a hydrophobic channel and (ii) a flat, positively charged surface. Non-specific membrane attachment is mediated by the charged surface and, once bound to the Golgi, it is postulated that an acyl group from an unknown Golgi protein is inserted into the hydrophobic channels of bet3, thus anchoring the protein specifically to this organelle (24). Whether bet3 alone is responsible for TRAPP anchoring to the Golgi is unclear. Recently, the crystal structure of a mammalian isoform of the Trs33 subunit was solved. It too formed homodimers, however, when mixed with purified bet3, could form a heterodimeric complex (26).

Although both TRAPP I and TRAPP II are found on the Golgi, biochemical and genetic evidence indicate that the two complexes function at different stages of the secretory pathway with TRAPP I acting in endoplasmic reticulum (ER)-to-Golgi traffic and TRAPP II acting in intra-Golgi traffic (14). The two yeast complexes have seven subunits in common (Bet5p, Bet3p, Trs20p, Trs23p, Trs31p, Trs33p and Trs85p), while TRAPP II also contains three unique subunits (Trs65p, Trs120p and Trs130p). Several pieces of evidence suggest that a thorough understanding of TRAPP architecture will lead to a better comprehension of TRAPP function. First, only TRAPP I, but not TRAPP II,

binds to ER-derived, COP II-coated vesicles (14), suggesting that the unique TRAPP II subunits somehow interfere with COP II-coated vesicle recognition. Second, while mammalian cells also contain orthologs of most of the subunits common to TRAPP I and TRAPP II (27,28), the only TRAPP II-specific subunit identified in database searches is a Trs130p ortholog (29). This suggests that the other TRAPP II-specific subunits are not well conserved and may indicate that the architecture of the complexes plays an important role in specifying the functional differences between TRAPP I and TRAPP II. Finally, while mutations in the ubiquitously expressed COG subunit, Cog7p, lead to pleiotropic developmental defects (30), mutations in the ubiquitously expressed TRAPP subunit trs20/sedlin specifically affect cartilage tissue (31–33). While the relatively mild phenotype associated with trs20 mutations may be partially explained by the presence of a processed pseudogene (34,35), it is also possible that the architecture of the TRAPP complexes or subunit interactions might differ among various tissues. To this end, our long-term goal is to fully elucidate the overall architecture of the complexes, as well as the structure of and the interactions between all the TRAPP subunits.

Here, we describe genetic and *in vitro* biochemical interactions between the yeast *Saccharomyces cerevisiae* TRAPP subunits, Bet3p and Trs33p. This interaction enabled another TRAPP subunit, Bet5p, to co-precipitate with Bet3p. We also present the crystal structure of the heterodimeric mammalian bet3–trs33 complex and show that trs33 is structurally similar to bet3. Genetic data on the yeast Trs33p suggest that several well-conserved basic residues are involved in mediating the interaction between Bet3p and (an)other protein(s). Our results indicate that Trs33p facilitates the Golgi-localization of Bet3p by mediating several of its protein–protein interactions in order to build the TRAPP complexes.

Results

Genetic interactions between bet3 and trs33 mutants

To begin to map TRAPP subunit interactions, we focused our attention on the subunits of the smaller TRAPP I complex (Bet5p, Bet3p, Trs20p, Trs23p, Trs31p, Trs33p and Trs85p). We previously described two specific yeast *bet3* mutations. One, in which both Lys24 and Lys96 are changed to Glu (*bet3-3*), removes a well-conserved, positively charged patch on the long flat surface of the Bet3p dimer. The second, in which residue Ala94 is changed to Leu (*bet3-4*), blocks the hydrophobic channel in the Bet3 protein, preventing the insertion of a potential Golgi-specific hydrophobic anchor (24). While the bet3-3 protein fails to bind to membranes, the bet3-4 protein localizes to multiple intracellular compartments (24). Of the seven TRAPP I subunits, the genes encoding two of the proteins (*TRS33* and *TRS85*) are nonessential for the vegetative growth of the cells (13,36). Whereas there are no reported growth defects for the *trs33*△, the *trs85*△ cells are extremely sick (36,37). Furthermore, *bet3-3* and *bet3-4* display no observable growth defects when grown at temperatures below 35 °C (not shown). Therefore, to begin our studies, we looked for a genetic interaction between the *bet3* mutants and *trs33*△.

Synthetic lethality is a genetic phenomenon that results when the combination of two mutations in a haploid cell leads to a lethal phenotype at temperatures where each individual mutation is viable (38). Such an interaction often indicates that the resulting gene products act at a common step of a pathway. We crossed a *trs33*△ strain with *bet3-3* and *bet3-4*, and then sporulated and dissected the tetrads. As shown in Figure 1A, all *trs33*△ *bet3-3* and *trs33*△ *bet3-4* spores were inviable at 25 °C. This genetic interaction between the *bet3* mutations and *trs33*△ is consistent with these two proteins being components of TRAPP. However, because neither of the *bet3* mutations displayed synthetic genetic interactions with *trs65*△ (Figure 1B), a disruption of the gene encoding another nonessential TRAPP subunit Trs65p, the genetic interaction between *bet3* and *trs33*△ is more specific and might indicate a measure of functional overlap or physical interaction between Bet3p and Trs33p.

It was previously reported that overexpression of *TRS33* can weakly suppress the temperature sensitive growth defect of a *bet3-1* mutant strain only at 30 °C, whereas overexpression of the genes encoding other TRAPP subunits could suppress the growth defect at higher temperatures (13). This mutation alters a conserved glycine residue along helix α2 of Bet3p and may interfere with the packing of helices α2 and α4 in the bet3-1 protein. We therefore examined whether overexpression of *TRS33* could also suppress the temperature sensitive growth phenotype of the *bet3-3* and *bet3-4* mutations. As shown in Figure 1C, overexpression of *TRS33* restores growth to the *bet3-3* and *bet3-4* mutations to near wild-type levels. On the basis of the differential ability of Trs33p to suppress the various *bet3* mutations (*bet3-1*, *bet3-3* and *bet3-4*), and the synthetic lethality described above, we conclude that Trs33p somehow assists in the function or membrane localization of Bet3p, perhaps through a direct protein–protein interaction between the two gene products.

The structure of the bet3-trs33 heterodimer

To test whether Bet3p and Trs33p physically interact, we expressed $(His)_6$-tagged recombinant forms of the yeast proteins in *Escherichia coli* for *in vitro* binding experiments. Although both proteins were highly expressed in the bacteria (Figure 2A, lanes 1 and 2), they were both insoluble (lanes 3 and 4). However, when co-expressed from a vector (pET-DUET) with two independent multiple cloning sites and T7 promotors upstream of both open-reading frames (ORF), the proteins were found to be highly expressed (lane 5) and soluble (lane 6) and could

be purified in a complex (lane 7) that migrated with the expected size of a 1:1 heterodimer, as judged using size exclusion chromatography (Figure 2B). This result suggests that recombinant Bet3p and Trs33p can indeed stably interact with each other.

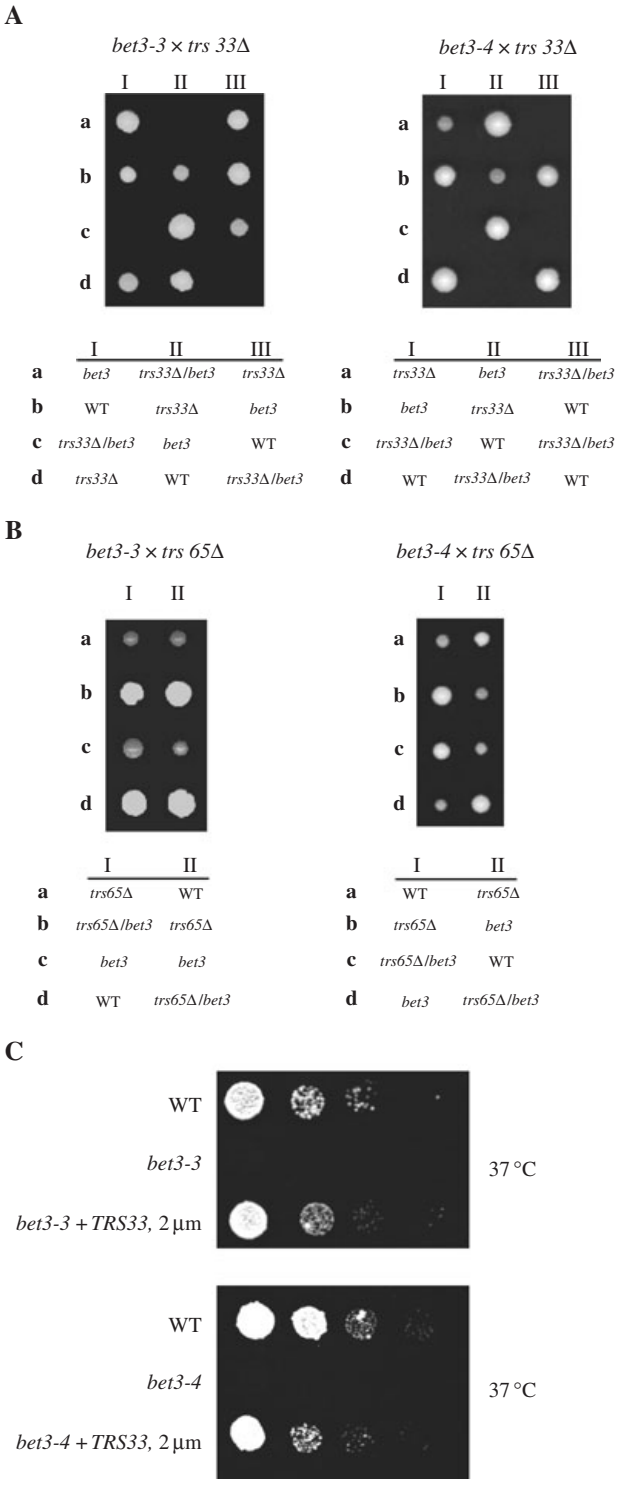

Figure 1: Genetic interactions between *BET3* and *TRS33*. (A) The *bet3-3* and *bet3-4* mutations are synthetically lethal with *trs33*△. The *bet3-3* (left panel) and *bet3-4* (right panel) strains were crossed to a *trs33*△ strain, sporulated and dissected. Three tetrads for each (I, II and II) are shown. The genotypes listed below each panel were determined by stamping onto dropout media and by scoring for auxotrophic markers. (B) The *bet3-3* and *bet3-4* mutations are not synthetically lethal with *trs65*△. The *bet3-3* (left panel) and *bet3-4* (right panel) strains were crossed to a *trs65*△ strain, sporulated and dissected. Two tetrads for each (I and II) are shown. The genotypes were as in panel A. (C) Overexpression of *TRS33* suppresses the *bet3-3* and *bet3-4* temperature sensitive growth defects. The *bet3-3* and *bet3-4* strains were transformed with *TRS33* on a *URA3*-based 2-μm vector (pRS426). Serial dilutions (10-fold) of wildtype (WT), *bet3-3* and *bet3-3* with *TRS33*-pRS426 (left panel) or WT, *bet3-4* and *bet3-4* with TRS33-pRS426 (right panel) were spotted onto YPD agar plates and incubated at 37 °C for 2 days. The small colonies in the tetrads contain the *ade2-1* mutation, known to slightly impede growth (56).

To examine the molecular basis for the Bet3p–Trs33p interaction, we sought to crystallize the complex. While the recombinant heterodimeric yeast complex was refractory to crystallization, a heterodimeric complex between recombinant full-length mouse bet3 (referred to as bet3) and recombinant full-length human trs33 (referred to as trs33) was identified that yielded crystals suitable for structure determination. The crystal structure of the complex was solved with multiple-wavelength anomalous dispersion (MAD) phasing using a crystal of selenomethionine-substituted proteins. In the final model, refined against data to 2.2 Å resolution, bet3 consists of residues 15-175, while trs33 consists of residues 2–19, 31–104 and 109–158. The missing segments are disordered in the crystal. Both structures are a mixed α/β-fold containing four α-helices and four β-strands, which form an antiparallel β-sheet (Figure 3A). While one face of the sheet exhibits extensive hydrophobic interactions with α3 and α4, the other face of the sheet is exposed to the bulk solvent. At the interface between the two subunits, the helices α1 and α2 of bet3 form a wedge-shaped binding groove for the binding of α1 of trs33. In an identical manner, the helices α1 and α2 of trs33 accepts α1 of bet3. The interactions between the helices are extensive and mostly hydrophobic, burying >15% of the total monomeric surface.

The structure reveals two completely unexpected features. First, bet3 and trs33 adopt a fold that is closely similar to each other. The Cα traces of the secondary structures of bet3 and trs33 can be superimposed with an r.m.s.d. value of 1.16 Å (Figure 3B). This was unexpected given the low homology between these two proteins (approximately 18%; see Figure 4A). Second, the two proteins form a 1:1 heterodimer, while bet3 expressed alone in *E. coli* forms a homodimer in both solution and in the crystals (24,25). In the structure of the bet3-trs33 heterodimer, the dimerization pattern

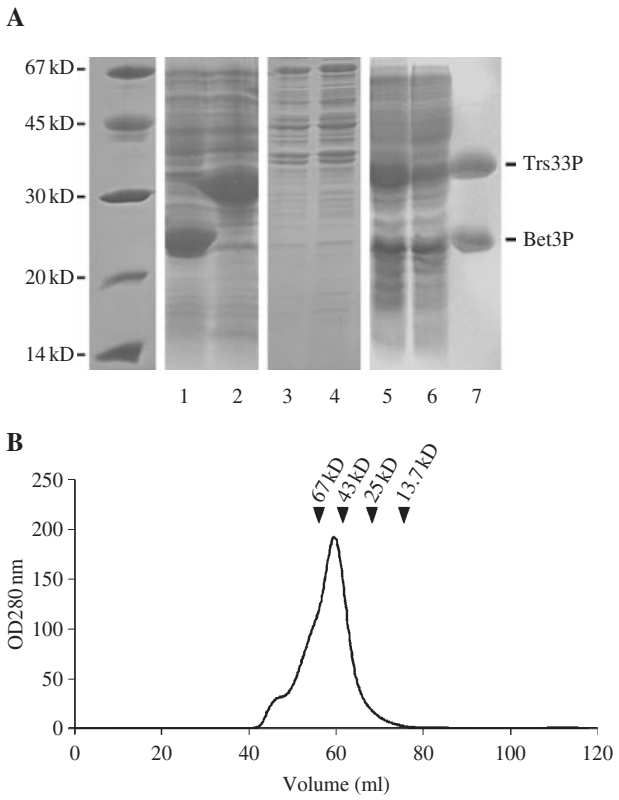

Figure 2: *In vitro* interactions between Bet3p and Trs33p. (A) Yeast TRAPP I subunits are insoluble. BL21(DE3) *Escherichia coli* cells bearing plasmids containing the open-reading frames for either Bet3p (lanes 1 and 3) or Trs33p (lanes 2 and 4) were induced with IPTG and lysed using sonication. Total lysates (lanes 1 and 2) and the soluble fraction following a 15 000 × *g* centrifugation (lanes 3 and 4) were fractionated using SDS–PAGE and stained with Coomassie Brilliant Blue. A plasmid containing both the *BET3* and *TRS33* open-reading frames was transformed into *E. coli* BL21(DE3) and grown at 37 °C to an OD600 = 1. IPTG was added to 1-mM final concentration, and the culture was grown for 18 h at 20 °C. The cells were pelleted and sonicated to produce a total cell lysate (lane 5). The lysate was centrifuged at 20 000 × *g* to produce the soluble fraction (lane 6). The soluble fraction was then incubated with Ni^{2+}-NTA to purify the Bet3p–Trs33p complex (lane 7). (B) Gel filtration analysis of the Bet3p–Trs33p complex. The Ni^{2+}-NTA-purified Bet3p–Trs33p complex was fractionated using size exclusion chromatography on a Sephadex 75 preparative column. Molecular weight standards, shown above the curve, were used to calibrate the size of the eluted complex, estimated to be approximately 51 000 Da. A minor high-molecular weight contaminant, seen as a shoulder on the main peak, was removed by this procedure.

observed in the bet3 structure is exactly preserved, and therefore, the heterodimeric complex looks as if one molecule of the bet3 homodimer is replaced by one molecule of trs33. One noticeable difference is that the symmetry-related pairing of the N-terminal β-strand (residues 12–16) in the bet3 homodimer (24,25) is absent in the bet3–trs33 complex. Such an interaction is impossible because trs33 is shorter than bet3 at the N-terminus and lacks a

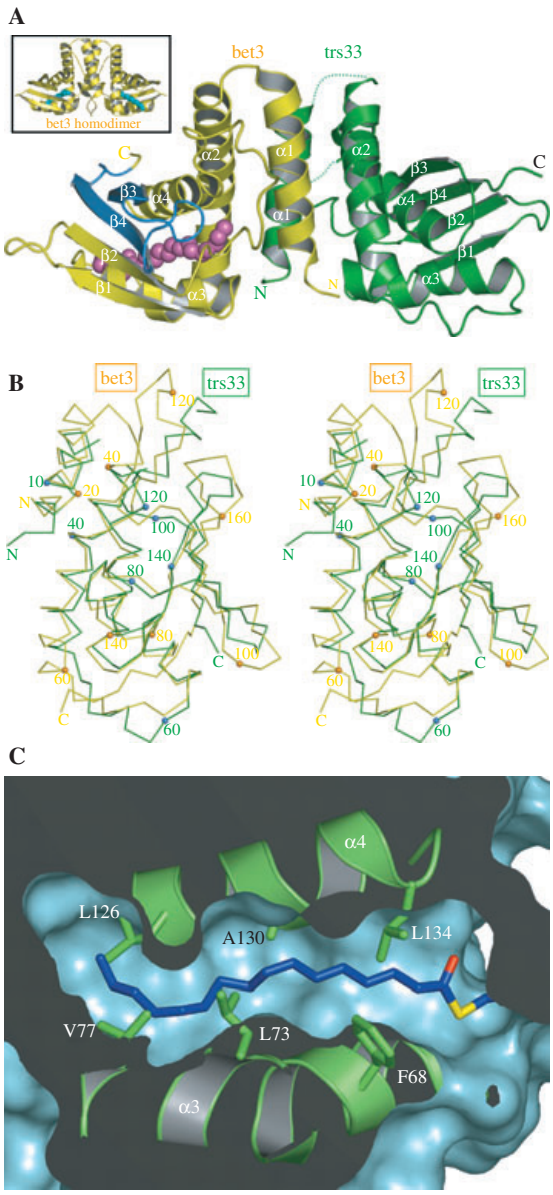

Figure 3: Structure of bet3–trs33 complex. (A) Ribbon representation of the bet3-trs33 heterodimer. bet3 and trs33 are colored in yellow and green, respectively. The secondary structures are numbered in the order of appearance in the primary sequence. Palmitoyl-Cys68 is a CPK model. Regions of loop α1-α2 (residues 20–30) and β2-α5 (residues 105–108) in trs33, whose electron density was missing, are presented as dotted lines. The inset figure shows the bet3 homodimer. The region of bet3 that shares limited homology with Dsl1p is colored in blue. (B) A stereo view of the superposition of the C_α traces of bet3 (yellow) and trs33 (green). The C_α atoms of a set of residues in bet3 (residues 17–30, 35–58, 71–91, 101–108, 127–150 and 161–168) and those in trs33 (residues 5–18, 31–5, 62–82, 91–98, 119–142 and 150–157) were superimposed with an r.m.s. deviation of 1.16 Å (for a total of 97 atoms). Every twentieth residue of bet3 and trs33 is indicated as numbered dots. (C) A cutaway view of the superposition in B showing the hydrophobic channel of bet3. The palmitoyl chain covalently linked to bet3 is in blue. Shown are the trs33 residues protruding into the space occupied by the palmitoyl chain. Phe68, Leu73, Leu126 and Leu134 are bulkier than the corresponding residues lining the channel of bet3 (see text).

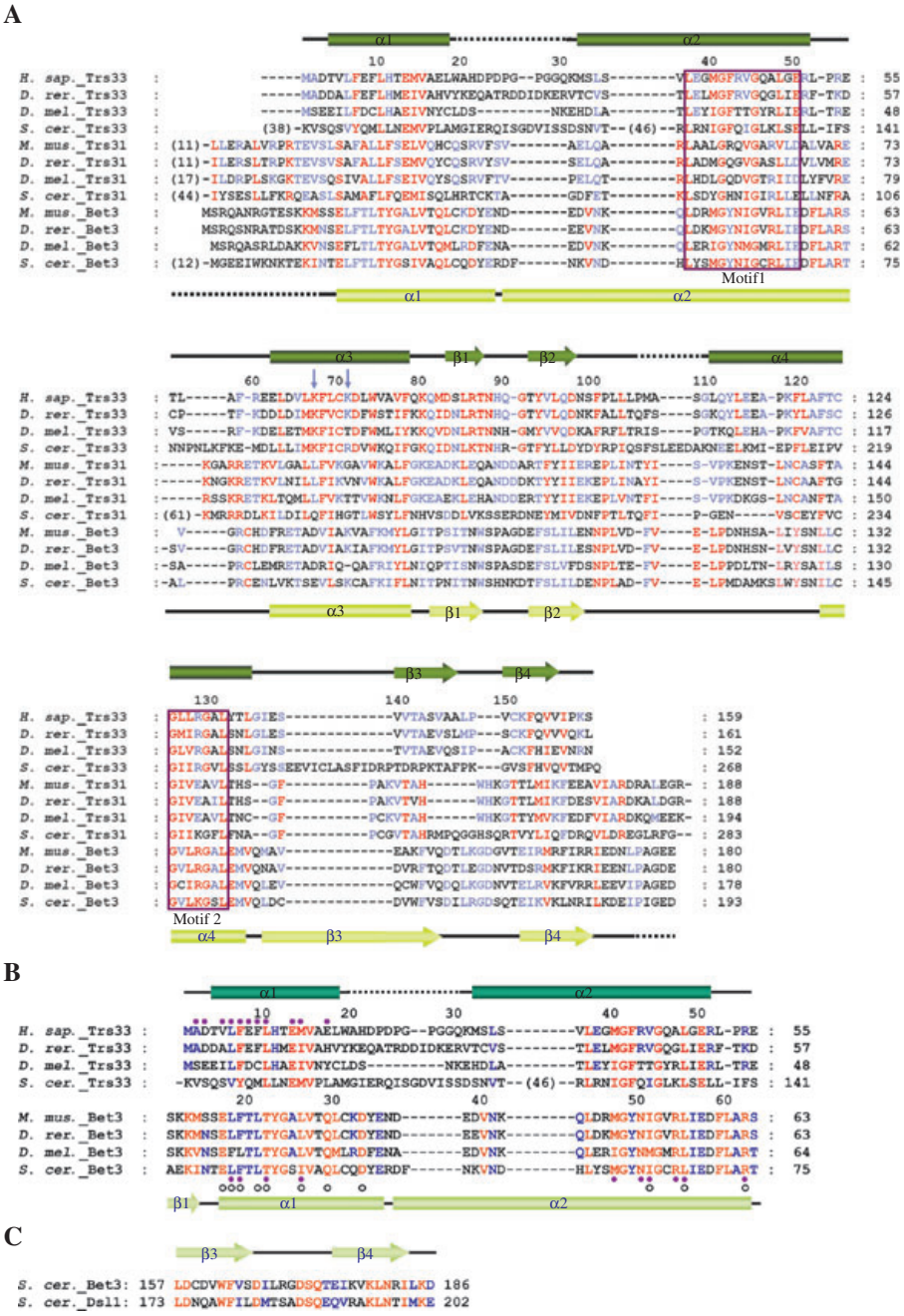

Figure 4: Sequence alignments of trs33, trs31 and bet3. (A) Secondary structural elements of trs33 and bet3 are indicated on the top and bottom of the alignment, respectively. The dotted lines indicate the disordered regions in the structure of the complex. The sequences of orthologs of bet3 and trs33 were aligned based on the structure comparison and then the sequences of trs31 orthologs were aligned to bet3 based on the sequence homology. Ten orthologs of each protein were aligned, and four of them are presented. The red and blue letters indicate the amino acids that are 100% and >80% conserved, respectively, in 10 representative orthologs of each protein. The purple boxes indicate conserved sequence motifs among the Bet3, Trs31 and Trs33 proteins (36). All of the conserved or invariant residues in these two motifs are involved in the intra- or intersubunit hydrophobic interactions. In particular, the invariant glycine residues, Gly41 and Gly45 on α2 and Gly125 and Gly129 on α4 (trs33 numbering), allow for an unusually close contact between the two α-helical backbones, such that substitution of any of these residues is likely to disrupt the structural integrity of the protein. The blue arrows indicate the conserved basic residues, which are mutated to glutamic acid residues in yeast Trs33p. (B) Sequence alignment of the N-terminal regions of trs33 and bet3. The secondary structural elements of trs33 and bet3 are indicated on the top and bottom of the alignment, respectively. Coloring is the same as in A. Filled circles above and below the alignment denote the residues of trs33 and bet3, respectively, that are involved in the heterodimer formation. Open circles denote the residues of bet3 involved in the formation of the bet3 homodimer. (C) Sequence alignment of a small region of homology between Bet3p and Dsl1p. Red and blue letters indicate identities and similarities, respectively.

polypeptide segment corresponding to residues 12–16 of bet3 (Figure 4A).

Absence of a hydrophobic channel in trs33

The structure of the bet3 homodimer revealed that the protein has a prominent hydrophobic channel lined by hydrophobic residues emanating mostly from α2, α3 and α4 (24,25). The channel was shown to fully accommodate myristoylated or palmitoylated Cys68 (24,25). In the structure of the bet3–trs33 complex, the hydrophobic channel of bet3 harbors the hydrocarbon chain of palmitoylated Cys68, as judged using the elongated electron density in the channel. In contrast, the corresponding region of the trs33 subunit does not have an accessible internal channel. The absence of the channel appears to arise from two structural alterations. First, α3 and α4 are closer to each other in trs33 than in bet3, resulting in the restriction of available space for a channel. As a consequence, while the distance between the Ca atoms of Ile78 and Ala138 located in the middle of the channel in bet3 is 10.1 Å, the distance between the corresponding residues Leu69 and Ala130 of trs33 is 7.7 Å. Second, substitution of four channel-lining residues in bet3 with bulkier residues in trs33 (Val77→Phe68, Ala82→Leu73, Val134→Leu126 and Val142→Leu134) leaves no space for an internal channel (Figures 3C and 4A).

Comparison between the interfaces of the bet3 homodimer and the bet3-trs33 heterodimer

The interface in the bet3 homodimer is formed by twofold symmetry-related interactions involving α1 and α2 of each bet3 molecule. The bet3 homodimer shows a pattern of domain swapping such that β1 of one molecule is between β1 and α3 of the other molecule (24). The region containing β1 and the loop β1-α1 would contribute to the stabilization of the bet3 homodimer through both van der Waals interactions and several hydrogen bonds, while that region is unstructured in the bet3–trs33 complex as described above. Along helix α1 of bet3, five hydrophobic residues (Leu18, Phe19, Leu21, Leu26 and Leu30) and one polar residue (Thr22) make extensive contacts with the wedge-shaped hydrophobic groove formed by α1 and α2 on the other bet3 molecule (Figure 5A). At the terminal region of α1, the carboxylate side chain of Asp33 is hydrogen bonded to the OD1 group of Asp33 and the NE2 group of Gln29 of the other molecule. These hydrogen bonds are absent in the bet3–trs33 complex because the Asp33 residue is not conserved in trs33, and α1 of trs33 is shorter than α1 of bet3.

The intersubunit interactions of the bet3 homodimer are not simply reiterated at the interface between trs33 and bet3. Most apparently, the α1 of trs33 interacting with the α1-α2 wedge of bet3 is shorter than, and oriented differently from, the α1 of bet3 in the bet3 homodimer (Figures 5A,B). Secondly, α1 of trs33 is involved in more prominent polar interactions than that of bet3. These interactions are mediated by Asp3, Glu8 and Glu13, none of which are conserved in bet3 (Figures 4B and 5B). In addition, qualitative differences of hydrophobic interactions are also found. For example, the side chain of Leu10 on α1 fits tightly into a hydrophobic pocket formed by bet3 residues Phe19, Thr22, Leu26 and Met47. In comparison, the similar hydrophobic pocket composed of Phe19, Thr22 and Leu26 in the bet3 homodimer is occupied with Thr22 of bet3, which is less hydrophobic than a leucine residue (Figures 5A,B). This means that the hydrophobic pocket is more suitable for accepting Leu10 of trs33 than Thr22 of bet3. The interactions between α1 of bet3 and the α1-α2 wedge of trs33 also exhibit distinct differences from the corresponding interactions in the bet3 homodimer (data not shown).

When mammalian or yeast Bet3 protein is co-expressed with the corresponding trs33 protein, only a heterodimeric complex is seen, with no evidence of a bet3 homodimer. Taken together with the structural analysis above, this indicates that a bet3 monomer might have a higher affinity for trs33 than for another bet3 molecule. To see whether this is true, we expressed mammalian bet3 and trs33 individually in *E. coli* and mixed them *in vitro* to see whether a heterodimer might form. As shown in Figure 5C, the bet3 and trs33 homodimers migrate to distinct locations on native polyacrylamide gels (lanes 1 and 2, respectively). When co-expressed in *E. coli*, the heterodimer displays a mobility intermediate to that of each homodimer (lane 3), with no indication of either bet3 or trs33 homodimers. When the homodimers are mixed *in vitro*, there is a reduction in the intensity of both homodimer bands and the appearance of a bet3-trs33 heterodimer (lane 4). These data support the structural analysis suggesting that bet3 is more likely to form a heterodimer with trs33 than a homodimer.

Functional consequence of the Bet3p–Trs33p interaction

Given the fact that bet3 and trs33 can physically interact, we sought to determine the functional significance of this interaction. To this end, all seven of the yeast TRAPP I subunits were cloned into the vector pcDNA3.1(+) with and without a carboxy-terminal c-*myc* epitope tag. The resulting DNA was used in a coupled transcription/translation reaction (TnT) using a rabbit reticulocyte lysate to produce the untagged (Figure 6A, lanes 1–7) and tagged (lanes 8–14) proteins. When incubated with anti-c-*myc* antibody, only the tagged subunits could be precipitated onto protein A-sepharose beads (Figure 6A, lanes 1–14, compare upper panel with lower panel). We then performed the TnT reaction using Bet3p-*myc* and each of the untagged subunits to investigate which proteins interact with Bet3p. The highest affinity interaction was between Bet3p-*myc* and Trs33p (Figure 6A, lane 16). A reciprocal experiment, using Trs33p-*myc* and untagged Bet3p confirmed this interaction (Figure 6A, lane 18). A weaker interaction, visible only after a longer incubation

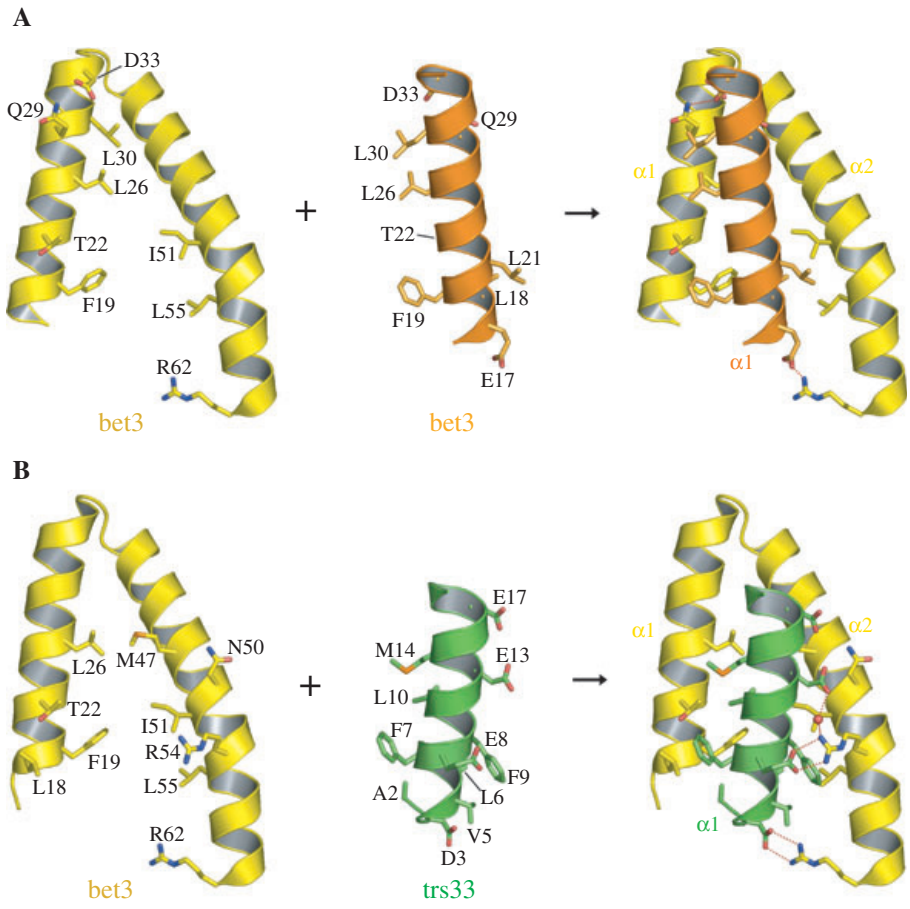

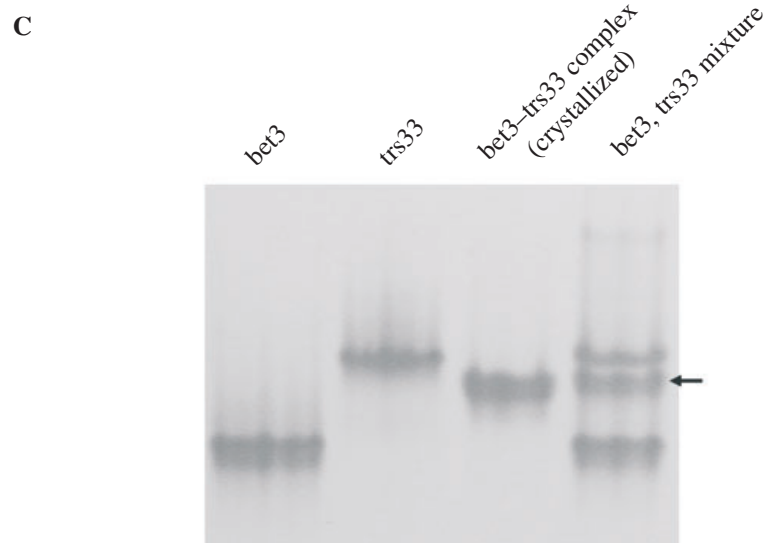

Figure 5: Interactions of the α1-α2 wedge of bet3 with α1 of bet3 or trs33. (A) The bet3–bet3 interaction. The two subunits of the bet3 homodimer are in different colors. (B) The bet3–trs33 interaction. The bet3 and trs33 polypeptides are in yellow and green, respectively. The red sphere represents a water molecule mediating hydrogen bonds. The α1-α2 groove of bet3 is oriented as in A. The residues involved in interactions closer than 3.9 Å are represented as ball-and-sticks in both A and B. A multiple anomalous dispersion electron density map of the bet3-trs33 interface region is available in supplemental materials at http://www.traffic.dk/suppmat/6_12a.asp. (C) *In vitro* formation of the bet3-trs33 heterodimer. Mouse bet3 (10 μM, lane 1) and human trs33 (10 μM, lane 2) were mixed together (lane 4) and incubated at 25 °C for 30 min and subjected to native gel electrophoresis. The arrow indicates the protein band that exhibits the same mobility as the bet3–trs33 complex purified from *Escherichia coli* and crystallized (lane 3).

time, was also seen between Bet3p-*myc* and Trs85p (not shown).

It was surprising that the only detected direct interactions with Bet3p were with nonessential gene products, because it is presumably necessary to anchor the essential Bet3p subunit into the TRAPP complex to ensure proper function. One possibility is that the Bet3p-Trs33p heterodimer might facilitate the interaction between Bet3p and other essential TRAPP subunits. To address

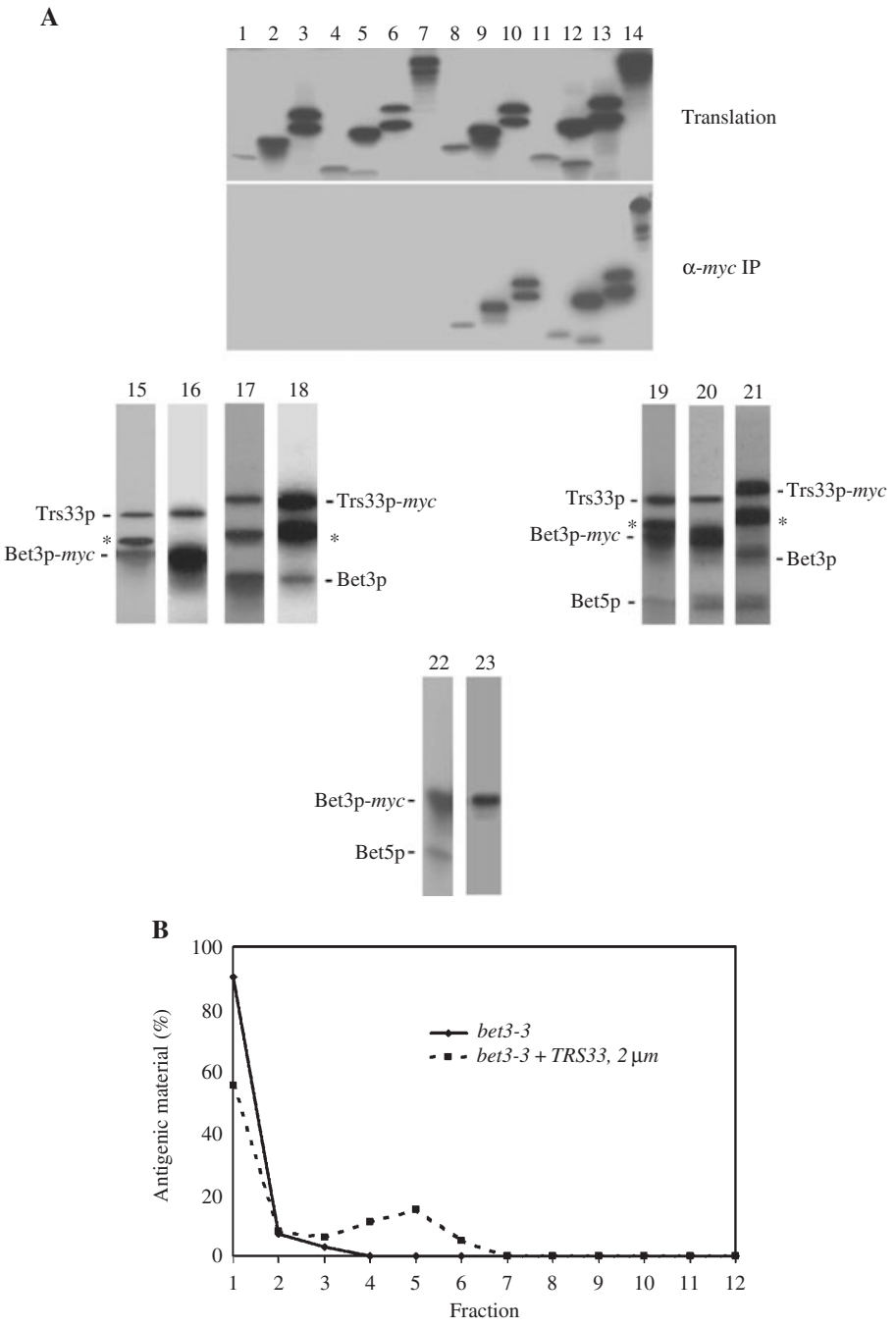

Figure 6: Functional consequence of the Bet3p–Trs33p interaction. (A) Trs33p facilitates a Bet3p–Bet5p interaction. Coupled *in vitro* transcription/translation reactions were performed as described in the *Materials and Methods*. Translation products of the untagged (lanes 1–7) and the *myc*-tagged (lanes 8–14) subunits were fractionated using SDS–PAGE. The order of the subunits in both the untagged and tagged lanes is Trs20p (lanes 1 and 8), Bet3p (lanes 2 and 9), Trs31p (lanes 3 and 10), Bet5p (lanes 4 and 11), Trs23p (lanes 5 and 12), Trs33p (lanes 6 and 13) and Trs85p (lanes 7 and 14). Internal initiation products are visible for Trs31p, Trs23p and Trs33p. Samples following immunoprecipitation with the anti-*myc* antibody are shown in the lower panel. The remaining reactions contained Bet3p-*myc* with Trs33p (lanes 15 and 16), Trs33p-*myc* with Bet3p (lanes 17 and 18), Bet3p-*myc* with Trs33p and Bet5p (lanes 19 and 20), Trs33p-*myc* with Bet3p and Bet5p (lane 21) and Bet3p-*myc* with Bet5p (lanes 22 and 23). The band marked by an asterisk (*) in lanes 15, 17, 18, 19 and 21 represents a truncated form of Trs33p produced by initiation at an internal methionine. This truncated Trs33p polypeptide does not bind to Bet3p, because it fails to precipitate with Bet3p-*myc* (compare lane 15 with lane 16 and lane 19 with lane 20). A sample of the reaction before immunoprecipitation is shown in lanes 15, 17, 19 and 22. (B) Trs33p increases the pool of Golgi-bound Bet3p. Lysates from 400 OD_{600} units of cells from both bet3-3 and bet3-3-overproducing TRS33 (the mutant bet3-3 protein is tagged with an HA epitope) were prepared and subjected to sucrose gradient fractionation as described in *Materials and Methods*. Fractions were collected from the top of the gradient and the bet3-3 protein from the mutant strain (solid line), and the strain overproducing TRS33 (dashed line) was identified by Western analysis using anti-HA antibody.

this question, we performed TnT reactions in which tagged and untagged Bet3p and Trs33p were co-expressed with the other TRAPP I subunits. Indeed, under these conditions, we now were able to observe the co-precipitation of Bet5p (Figure 6A, lanes 20 and 21). We were unable to detect a Bet3p interaction with Bet5p in the absence of Trs33p (Figure 6A, lane 23). These results show that, *in vitro*, Bet3p can interact with Trs33p, and this interaction facilitates the interaction between Bet3p and Bet5p.

Because the yeast Trs33 protein facilitates the interaction between Bet3p and Bet5p, we speculated that Trs33p might facilitate the Golgi-localization of Bet3p. To examine this, we used the *bet3-3* mutant to determine whether Trs33p can increase the amount of Bet3p on Golgi membranes. Sucrose gradients were used in which Golgi proteins are well-documented to migrate in fractions 4–7, while soluble proteins remain at the top of the gradient in fraction 1 (21,39,40). As previously reported (24) and shown in Figure 6B (solid line), the bet3–3 protein fails to enter the sucrose gradients to any significant degree. Thus, the protein is largely found in the soluble fraction. However, when *TRS33* is overproduced in the *bet3-3* mutant cells, a significant amount of the bet3–3 protein is now found in fractions 4–6. These results show that Trs33p is capable of driving Bet3p to Golgi membranes.

The Trs33p-mediated increase of Golgi-bound Bet3p is likely due to the physical interaction between these two proteins as described above. One possibility is that Trs33p may provide the basic residues that the mutant bet3-3 protein is lacking. A multiple sequence alignment suggests that there are indeed well-conserved, basic residues including Lys67 and Lys71 on trs33 (equivalent to Lys158 and Arg162 in yeast Trs33p; Figure 4A) found on the flat surface of the dimer from which they were replaced to produce *bet3-3*. To begin to address whether these basic residues assisted in Bet3p membrane localization, we mutated them in the yeast Trs33 protein to glutamic acid [Trs33p(K158/R162E)] and tested the ability of this mutated version of Trs33p to suppress the temperature sensitive growth of the *bet3-3* and *bet3-4* strains. Interestingly, overexpression of Trs33p(K158/R162E) could only suppress the temperature sensitive growth defect of the charge-inverted *bet3-3* mutation but not that of the channel-blocked *bet3-4* mutation (not shown). This result suggests that Lys158 and/or Arg162 in Trs33p do not functionally substitute for either Lys24 or Lys96 of Bet3p. Because wildtype Trs33p can suppress the *bet3-4* mutation, this result also suggests that the mutated residues in Trs33p are somehow involved in the anchoring of Bet3p to an acyl moiety. Given the distance between these residues and the Bet3p hydrophobic channel, this event is probably achieved by a Trs33p-mediated protein–protein interaction involving a third protein.

Discussion

With 7–10 distinct polypeptides present in multiple copies, understanding the role of each TRAPP subunit and its interactions within the complex will be a difficult task. Our approach has been to reduce the complex to its individual components and to solve the three-dimensional crystal structure of the proteins to achieve a better understanding of the function of the subunits. This has been done for two of the subunits (24,41), and we now report the beginning of the next phase, which is elucidating the structure and function of heteromeric complexes between TRAPP subunits.

Our genetic data suggested a potential interaction between Bet3p and Trs33p, which was borne out in several different *in vitro* systems (Figures 2A, 5C and 6A). We previously reported that recombinant mammalian bet3 and trs33 could not interact *in vitro* (24). In that study, mouse trs33 was used, but the protein was likely misfolded as judged using size exclusion chromatography and native gel electrophoresis, thus explaining the lack of interaction. In this study, we produced human trs33 as an MBP-fusion protein and were able to obtain small amounts of properly folded protein for the *in vitro* binding study (Figure 5C). The present work shows that one of the functions of Trs33p is to mediate the interaction between the essential TRAPP subunits Bet3p and Bet5p. This physical interaction is consistent with genetic data that identified the *BET5* gene as a suppressor of the *bet3-1* mutant phenotype (42). Our inability to detect Bet3p interactions directly with other essential TRAPP subunits *in vitro* can be explained in several ways. First, these interactions may not be of high enough affinity to detect using the TnT system. Second, Bet3p might interact with heteromers of essential TRAPP subunits and not monomers. Finally, these interactions may be mediated by other cellular components that are missing in the TnT system. It is noteworthy that we can co-express and purify a heterodimeric Bet3p–Trs31p complex from *E. coli* but did not see any evidence of this complex in the TnT system (CM, JW, MC and MS, unpublished observation). Therefore, it appears that the mapping of interactions in a multiprotein complex such as TRAPP will have to rely on several different methodologies.

Given the complex nature of TRAPP and, as stated above, the interactions seen between recombinant Bet3p and other TRAPP subunits in *E. coli*, it is difficult to estimate to what extent the Bet3 protein is involved in homo- versus heterodimeric interactions. It is possible that these could change with the absolute concentration of the proteins in the cell. Furthermore, Turnbull et al. (2005) estimate a dissociation constant for the bet3 homodimer of approximately 450 nM and suggest that homodimers may only be present in compartments that are enriched in the Bet3 protein. We have presented structural and biochemical evidence suggesting that bet3-trs33

heterodimers might be the prevalent species in cells. Consistent with this notion, we were unable to detect Bet3p or Trs33p homodimers using the TnT system or when co-expressed in *E. coli* but could readily detect the heterodimer in both systems. Therefore, it is possible that both Bet3 and Trs33 homodimers may not exist at all *in vivo*, and only heterodimers of these proteins may be found. This would be similar to what was reported for calpain, where strictly heterodimers of the catalytic and regulatory subunits are found *in vivo* but homodimers of a portion of the regulatory subunit can be produced and crystallized (43). In yeast, *TRS33* is nonessential. Given the nearly identical fold shared between Bet3p and Trs33p, and the overall similarity between the bet3 homodimer and the bet3-trs33 heterodimer, we speculate that in the absence of Trs33p, a Bet3p homodimer could substitute for the heterodimer, thus explaining the nonessential nature of *TRS33*.

Although related over a very limited number of residues at the amino acid level (36), trs33 and bet3 are structurally similar. Solving the structures of the remaining TRAPP subunits will shed light on whether this phenomenon can be extended to other TRAPP components. Using an iterative PSI-BLAST search, Whyte and Munro reported previously hidden identities at the amino acid level between subunits of the exocyst, COG and GARP complexes (44), and suggested that portions of components of vesicle-tethering factors may be distantly related. The crystal structure of the bet3–trs33 complex reported here as well as that of the trs33 homodimer (26) supports this contention between subunits of the same complex and shows that whole subunits may be structurally related. Interestingly, it has been shown by sequence analysis that several TRAPP subunits share regions of significant homology (36,45), perhaps indicating some structural and/or functional overlap amongst those subunits. Furthermore, Bet3p shares a small region of homology with Dsl1p (see Figures 3 and 4C), a protein involved in a Golgi-to-ER retrograde-trafficking complex (46,47). This homology is restricted to the β4-loop-β5 surface-exposed region of Bet3p, suggesting this region may be involved in an analogous function between the proteins. The significance of these sequence analyses will become clearer as the structures of other subunits in the various complexes are reported.

Heinemann and colleagues (26) recently reported the crystal structure of a human trs33 isoform (accession code AL833179, isoform I), which is 56% identical to the trs33 isoform investigated here (accession code AAC62259, isoform II). The polypeptide fold of trs33 isoform I, solved as a homodimer, is essentially identical to the fold of trs33 isoform II in the bet3-trs33 heterodimer presented here. Their data reinforce our conclusion that bet3 and trs33 could form homodimers in the absence of either protein, but the heterodimer is the functional unit. In the presence of a crosslinker, they too observed formation of a bet3-trs33 heterodimer *in vitro* following mixing of homodimers of the proteins. In contrast, the bet3–trs33 complex was readily formed in our reaction without the need for a crosslinker. A likely explanation for the differences in the stability of the heterodimers lies in the amino acid differences between the isoforms. Six of the trs33 isoform II residues interacting with bet3 differ from those in isoform I used by Heinemann and colleagues. These are Val5→Ala5, Glu8→Leu8, Phe9→Leu9, Glu17→Gly17, Val36→Lys35 and Ala47→Gly46. Given the detailed interactions we presented between bet3 and trs33 (Figure 5B), all of the substitutions are expected to reduce the affinity of trs33 isoform I for bet3. The functional significance of the presence of trs33 isoforms is not known. However, the extreme difficulty in the production of trs33 isoform II as a soluble homodimer and its prompt formation of the heterodimer with bet3 *in vitro* suggest that this isoform might be the one that is incorporated into TRAPP complexes in mammalian cells. The biological role of the other isoform is not clear.

Materials and Methods

Transcription/translation reactions

The ORFs encoding the yeast TRAPP I subunits were amplified using PCR with or without a c-*myc* epitope tag at the carboxy-terminus and cloned into pCDNA3.1(+). DNA was transcribed and translated using the TnT® system (Promega, Madison, WI, USA) according to the manufacturer's instructions. Samples were diluted 50-fold with HENT buffer (20 mM HEPES, pH 7.5; 1 mM EDTA; 150 mM NaCl and 0.5% Triton-X-100), incubated on ice for 1–18 h and centrifuged at 13 000 × *g* for 5 min. The samples were transferred to fresh tubes and incubated with 4 μg anti-c-*myc* IgG (Upstate, Lake Placid, NY, USA) for 1 h on ice before adding protein A-sepharose beads (Sigma, St Louis, MO, USA). The incubation was continued at 4 °C for an additional hour before washing the beads three times with HENT. Samples were boiled in SDS–PAGE sample buffer, resolved by SDS–PAGE and exposed to X-ray film.

Yeast strain construction and genetic analyses

Standard yeast manipulations, growth media and genetic analyses were as described (48).

Construction and expression of recombinant yeast proteins

The ORFs of yeast *BET3* and *TRS33* were obtained using PCR amplification and ligated into the BglII/XhoI site (for *BET3*) and the BamHI/SalI site (for *TRS33*) of a modified version of the dual expression vector pETDUET-1 (49). Constructs were transformed into the BL21(DE3) strain of *E. coli* for testing of expression and solubility as follows. The cultures were grown to an OD600 of approximately 1, and recombinant protein production was initiated by addition of 1 mM isopropyl-D-thiogalactopyranoside (IPTG). The cells were grown overnight at 20 °C, harvested and lysed using sonication. Lysates were separated into supernatant and pellet fractions by centrifugation at 20 000 × *g* for 20 min. The supernatant fraction was purified by Ni-NTA chromatography according to standard protocols.

Construction and expression of recombinant mammalian proteins

The mouse bet3 and the human trs33 (gi:3688090) genes were amplified using PCR and ligated into the pProExHTa (Invitrogen, Carlsbad, CA, USA) vector. A two-promoter expression vector containing the coding sequences for full-length bet3 and trs33 was constructed, in which the two genes were under the control of Trc promoter and T7 promoter, respectively. The two proteins were produced in *E. coli* BL21(DE3).

Table 1: Data collection, phasing and refinement statistics

	bet3-trs33	SeMet-bet3-trs33		
Data collection				
Space group	P212121	P212121		
Cell dimensions a, b and c (Å)	52.88, 70.52, 88.97	52.97, 70.89, 89.12		
		Peak	Inflection	Remote
Wavelength	1.00000	0.97989	0.98000	0.97130
Resolution (Å)		30.0–3.0	30.0–2.8	30.0–2.8
R_{sym}[a]		7.2 (44.3)	4.9 (33.6)	5.2 (35.0)
$I/\sigma I$		29.8 (3.8)	32.7 (3.4)	36.3 (4.5)
Completeness (%)		92.4 (89.2)	92.2 (87.4)	73.8 (80.1)
Redundancy		3.8	4.4	7.8
Refinement				
Resolution (Å)	10.0–2.2			
Number of reflections[b]	15881			
R_{work}/R_{free}	21.9/23.7			
Number of atoms				
Protein	2419			
Ligand/ion	0			
Water	65			
B-factors				
Protein	30.4			
Ligand/ion				
Water	31.47			
R.m.s. deviations				
Bond lengths (Å)	0.00678			
Bond angles (°)	1.17508			
Ramachandran plot (%)				
Most favored region	93.2			
Additionally allowed region	6.4			
Generously allowed region	0.4			

[a]Values in parentheses are for the highest resolution shell.
[b]Reflections of $|F_{obs}| > 1.0\ \sigma$.

Expression of the proteins was induced by 1 mM IPTG at an OD600 of 0.5 at 18 °C and incubated overnight. Bacterial lysates were prepared using sonication in buffer A, containing 20 mM Tris–HCl (pH 8.0) and 5 mM β-mercaptoethanol. The supernatant of the cell lysates following centrifugation was loaded onto a Ni-NTA column (Qiagen, Valencia, CA, USA) and eluted with buffer A containing 300 mM imidazole. The eluted solution was loaded onto a Hitrap Q anion exchange column (Amersham Biosciences, Princeton, NJ, USA). The N-terminal $(His)_6$-tag attached to bet3 was removed using TEV protease, and the reaction mixture was loaded onto an Ni-NTA column from which the bet3–trs33 complex was present in the flow through fraction. The complex was further purified with a Hitrap Q column (Amersham Biosciences). The fraction containing the bet3–trs33 complex was concentrated to 35 mg/mL in 20 mM Tris–HCl (pH 8.0) buffer containing 3 mM DTT and used for crystallization. Selenomethionine-substituted bet3–trs33 complex was produced in the *E. coli* B834(DE3) methionine auxotroph (Novagen, Madison, WI, USA) and purified as described above.

Crystallization and structure determination

Crystals of the bet3–trs33 complex were obtained by the hanging-drop vapor-diffusion method at 12 °C by mixing and equilibrating 3 μL of each of the protein solution with a precipitant solution containing 0.2 M ammonium formate and 28% polyethylene glycol (PEG) 3350. To obtain larger crystals, we subsequently transferred the initial crystals to a 1:1 mixture (v/v) of the protein solution and the reservoir solution containing 0.1 M ammonium formate and 26% PEG 3350. The crystals belonged to the space group $P2_12_12_1$ with the unit cell dimensions of a = 52.88, b = 70.52 and c = 89.97 and contained one heterodimer in the asymmetric unit. MAD data set was collected with a crystal of selenomethionine-substituted bet3-trs33 on the beamline BL41XU at Spring-8 in Japan. Thirteen selenium sites in the asymmetric unit were located and used for phase determination at 2.8 Å with the program SOLVE (50), and phases were subsequently improved by density modification with the program RESOLVE (51). The model building and refinement was performed with the programs O (52) and CNS (53), respectively, with 2.2 Å native data collected on beamline 6B at the Pohang Accelerator Laboratory, Korea. All diffraction data were processed using the programs DENZO and SCALEPACK (54). The position of bet3 was determined by the molecular replacement method with the CCP4 version of AmoRe (55) using the previously reported structure of bet3 (24). Crystallographic data statistics are summarized in Table 1.

Sucrose gradient fractionation

Preparation of lysates from 400 OD_{600} units of cells and sucrose gradient fractionation was as described (21). Western analysis was performed with anti-HA antibody (1:2000 dilution; Covance, Berkeley, CA, USA) and goat anti-mouse-HRP (1:5000 dilution; Santa Cruz Biotechnology, Santa Cruz, CA, USA).

Coordinates

The coordinates of the bet3-trs33 structure have been deposited in the Protein Data Bank with the code 2C0J.

Acknowledgments

This work was supported by funding from Genome Canada, Genome Quebec, the National Research Council of Canada and Creative Research

Initiatives of the Korean Ministry of Science & Technology. This study made use of the beamlines BL41XU at Spring-8 in Japan and .6B at the Pohang Accelerator Laboratory in Korea. K-HL and Y-GK were supported by the Brain Korea 21 Project.

References

1. Gillingham AK, Munro S. Long coiled-coil proteins and membrane traffic. Biochim Biophys Acta 2003;1641:71–85.
2. Guo W, Sacher M, Barrowman J, Ferro-Novick S, Novick P. Protein complexes in transport vesicle targeting. Trends Cell Biol 2000;10:251–255.
3. Lupashin V, Sztul E. Golgi tethering factors. Biochim Biophys Acta 2005, 1744, 325–339.
4. Oka T, Krieger M. Multi-component protein complexes and Golgi membrane trafficking. J Biochem (Tokyo) 2005;137:109–114.
5. Whyte JR, Munro S. Vesicle tethering complexes in membrane traffic. J Cell Sci 2002;115:2627–2637.
6. Terbush DR, Maurice T, Roth D, Novick P. The Exocyst is a multiprotein complex required for exocytosis in Saccharomyces cerevisiae. EMBO J 1996;15:6483–6494.
7. Conibear E, Stevens TH. Vps52p, Vps53p, and Vps54p form a novel multisubunit complex required for protein sorting at the yeast late Golgi. Mol Biol Cell 2000;11:305–323.
8. Conibear E, Cleck JN, Stevens TH. Vps51p mediates the association of the GARP (Vps52/53/54) complex with the late Golgi t-SNARE Tlg1p. Mol Biol Cell 2003;14:1610–1623.
9. Ungar D, Oka T, Brittle EE, Vasile E, Lupashin VV, Chatterton JE, Heuser JE, Krieger M, Waters MG. Characterization of a mammalian Golgi-localized protein complex, COG, that is required for normal Golgi morphology and function. J Cell Biol 2002;157:405–415.
10. Peterson MR, Emr SD. The class C Vps complex functions at multiple stages of the vacuolar transport pathway. Traffic 2001;2:476–486.
11. Rieder SE, Emr SD. A novel RING finger protein complex essential for a late step in protein transport to the yeast vacuole. Mol Biol Cell 1997;8:2307–2327.
12. Seals DF, Eitzen G, Margolis N, Wickner WT, Price A. A Ypt/Rab effector complex containing the Sec1 homolog Vps33p is required for homotypic vacuole fusion. Proc Natl Acad Sci USA 2000;97:9402–9407.
13. Sacher M, Jiang Y, Barrowman J, Scarpa A, Burston J, Zhang L, Schieltz D, Yates JR III, Abeliovich H, Ferro-Novick S. TRAPP, a highly conserved novel complex on the cis-Golgi that mediates vesicle docking and fusion. EMBO J 1998;17:2494–2503.
14. Sacher M, Barrowman J, Wang W, Horecka J, Zhang Y, Pypaert M, Ferro-Novick S. TRAPP I implicated in the specificity of tethering in ER-to-Golgi transport. Mol Cell 2001;7:433–442.
15. Guo W, Roth D, Walch-Solimena C, Novick P. The exocyst is an effector for Sec4p, targeting secretory vesicles to sites of exocytosis. EMBO J 1999;18:1071–1080.
16. Siniossoglou S, Pelham HR. An effector of Ypt6p binds the SNARE Tlg1p and mediates selective fusion of vesicles with late Golgi membranes. EMBO J 2001;20:5991–5998.
17. Suvorova ES, Duden R, Lupashin VV. The Sec34/Sec35p complex, a Ypt1p effector required for retrograde intra-Golgi trafficking, interacts with Golgi SNAREs and COPI vesicle coat proteins. J Cell Biol 2002;157:631–643.
18. Wang W, Sacher M, Ferro-Novick S. TRAPP stimulates guanine nucleotide exchange on Ypt1p. J Cell Biol 2000;151:289–296.
19. Wurmser AE, Sato TK, Emr SD. New component of the vacuolar class C-Vps complex couples nucleotide exchange on the Ypt7 GTPase to SNARE-dependent docking and fusion. J Cell Biol 2000;151:551–562.
20. Kim DW, Massey T, Sacher M, Pypaert M, Ferro-Novick S. Sgf1p, a new component of the Sec34p/Sec35p complex. Traffic 2001;2:820–830.
21. Barrowman J, Sacher M, Ferro-Novick S. TRAPP stably associates with the Golgi and is required for vesicle docking. EMBO J 2000;19:862–869.
22. Finger FP, Hughes TE, Novick P. Sec3p is a spatial landmark for polarized secretion in budding yeast. Cell 1998;92:559–571.
23. Lee MC, Miller EA, Goldberg J, Orci L, Schekman R. Bi-directional protein transport between the ER and Golgi. Annu Rev Cell Dev Biol 2004;20:87–123.
24. Kim YG, Sohn EJ, Seo J, Lee KJ, Lee HS, Hwang I, Whiteway M, Sacher M, Oh BH. Crystal structure of bet3 reveals a novel mechanism for Golgi localization of tethering factor TRAPP. Nat Struct Mol Biol 2005;12:38–45.
25. Turnbull AP, Kummel D, Prinz B, Holz C, Schultchen J, Lang C, Neiser FH, Hofmann KP, Jaresch E, Sommer T, Heinemann U. Structure of palmitoylated BET3: insights into TRAPP complex assembly and membrane localization. EMBO J 2005;24:875–884.
26. Kummel D, Muller JJ, Roske Y, Misselwitz R, Bussow K, Heinemann U. The structure of the TRAPP subunit TPC6 suggests a model for a TRAPP subcomplex. EMBO Rep 2005;6:787–793.
27. Gavin AC, Bosche M, Krause R, Grandi P, Marzioch M, Bauer A, Schultz J, Rick JM, Michon AM, Cruciat CM, Remor M, Hofert C, Schelder M, Brajenovic M, Ruffner H. Functional organization of the yeast proteome by systematic analysis of protein complexes. Nature 2002;415:141–147.
28. Sacher M, Ferro-Novick S. Purification of TRAPP from Saccharomyces cerevisiae and identification of its mammalian counterpart. Methods Enzymol 2001;329:234–241.
29. Loh E, Peter F, Subramaniam NV, Hong W. Mammalian Bet3 functions as a cytosolic factor participating in transport from the ER to the Golgi apparatus. J Cell Sci 2005;118:1209–1222.
30. Wu X, Steet RA, Bohorov O, Bakker J, Newell J, Krieger M, Spaapen L, Kornfeld S, Freeze HH. Mutation of the COG complex subunit gene COG7 causes a lethal congenital disorder. Nat Med 2004;10:518–523.
31. Gedeon AK, Colley A, Jamieson R, Thompson EM, Rogers J, Sillence D, Tiller GE, Mulley JC, Gecz J. Identification of the gene (SEDL) causing X-linked spondyloepiphyseal dysplasia tarda. Nat Genet 1999;22:400–404.
32. Sacher M. Membrane traffic fuses with cartilage development. FEBS Lett 2003;550:1–4.
33. Savarirayan R, Thompson E, Gecz J. Spondyloepiphyseal dysplasia tarda (SEDL, MIM #313400). Eur J Hum Genet 2003;11:639–642.
34. Gecz J, Hillman MA, Gedeon AK, Cox TC, Baker E, Mulley JC. Gene structure and expression study of the SEDL gene for spondyloepiphyseal dysplasia tarda. Genomics 2000;69:242–251.
35. Ghosh AK, Majumder M, Steele R, White RA, Ray RB. A novel 16-kilodalton cellular protein physically interacts with and antagonizes the functional activity of c-myc promoter-binding protein 1. Mol Cell Biol 2001;21:655–662.
36. Sacher M, Barrowman J, Schieltz D, Yates JR III, Ferro-Novick S. Identification and characterization of five new subunits of TRAPP. Eur J Cell Biol 2000;79:71–80.
37. Kaytor MD, Livingston DM. GSG1, a yeast gene required for sporulation. Yeast 1995;11:1147–1155.
38. Guarente L. Synthetic enhancement in gene interaction. a genetic tool come of age. Trends Genet 1993;9:362–366.
39. Otte S, Belden WJ, Heidtman M, Liu J, Jensen ON, Barlowe C. Erv41p and Erv46p: new components of COPII vesicles involved in transport between the ER and Golgi complex. J Cell Biol 2001;152:503–518.
40. Schroder S, Schimmoller F, Singer-Kruger B, Riezman H. The Golgi-localization of yeast Emp47p depends on its di-lysine motif but is not affected by the ret1-1 mutation in alpha-COP. J Cell Biol 1995;131:895–912.

41. Jang SB, Kim YG, Cho YS, Suh PG, Kim KH, Oh BH. Crystal structure of SEDL and its implications for a genetic disease spondyloepiphyseal dysplasia tarda. J Biol Chem 2002;277:49863–49869.
42. Jiang Y, Scarpa A, Zhang L, Stone S, Feliciano E, Ferro-Novick S. A high copy suppressor screen reveals genetic interactions between BET3 and a new gene. Evidence for a novel complex in ER-to-Golgi transport. Genetics 1998;149:833–841.
43. Blanchard H, Li Y, Cygler M, Kay CM, Simon J, Arthur C, Davies PL, Elce JS. Ca (2+)-binding domain VI of rat calpain is a homodimer in solution: hydrodynamic, crystallization and preliminary X-ray diffraction studies. Protein Sci 1996;5:535–537.
44. Whyte JR, Munro S. The Sec34/35 Golgi transport complex is related to the exocyst, defining a family of complexes involved in multiple steps of membrane traffic. Dev Cell 2001;1:527–537.
45. Ethell IM, Hagihara K, Miura Y, Irie F, Yamaguchi Y. Synbindin, A novel syndecan-2-binding protein in neuronal dendritic spines. J Cell Biol 2000;151:53–68.
46. Andag U, Schmitt HD. Dsl1p, an essential component of the Golgi-endoplasmic reticulum retrieval system in yeast, uses the same sequence motif to interact with different subunits of the COPI vesicle coat. J Biol Chem 2003;278:51722–51734.
47. Reilly BA, Kraynack BA, VanRheenen SM, Waters MG. Golgi-to-endoplasmic reticulum (ER) retrograde traffic in yeast requires Dsl1p, a component of the ER target site that interacts with a COPI coat subunit. Mol Biol Cell 2001;12:3783–3796.
48. Guthrie C, Fink GR. Guide to Yeast Genetics and Molecular Biology. Academic Press, Inc.; San Diego, CA, USA; 1991.
49. Lunin VV, Munger C, Wagner J, Ye Z, Cygler M, Sacher M. The structure of the MAPK scaffold, MP1, bound to its partner, p14. A complex with a critical role in endosomal map kinase signaling. J Biol Chem 2004;279:23422–23430.
50. Terwilliger TC, Berendzen J. Automated MAD and MIR structure solution. Acta Crystallogr D Biol Crystallogr 1999;55:849–861.
51. Terwilliger TC. Maximum-likelihood density modification. Acta Crystallogr D Biol Crystallogr 2000;56 yu(8):965–972.
52. Jones TA, Zou JY, Cowan SW, Kjeldgaard M. Improved methods for building protein models in electron density maps and the location of errors in these models. Acta Crystallogr A 1991;47:110–119.
53. Brunger AT, Adams PD, Clore GM, DeLano WL, Gros P, Grosse-Kunstleve RW, Jiang JS, Kuszewski J, Nilges M, Pannu NS, Read RJ, Rice LM, Simonson T, Warren GL. Crystallography & NMR system: a new software suite for macromolecular structure determination. Acta Crystallogr D Biol Crystallogr 1998;54:905–921.
54. Otwinowski Z, Minor W. Processing of X-ray diffraction data collected in oscillation mode. Methods Enzymol 1997;276:307–326.
55. CCP4, Collaborative Computational Project Number 4. The CCP4 suite: programs for protein crystallography. Acta Crystallogr 1994;D50:760–763.
56. Ugolini S, Bruschi CV. The red/white colony color assay in the yeast Saccharomyces cerevisiae: epistatic growth advantage of white ade8-18, ade2 cells over red ade2 cells. Curr Genet 1996;30:485–492.